

Article

Wear Model of Silicon Nitride Ceramic Balls in Three-Body Coupling Grinding Mode

Wei Yu ¹, Binghai Lv ^{2,*} and Julong Yuan ²¹ College of Electrical and Information Engineering, Quzhou University, Quzhou 324000, China² Key Laboratory of E&M, Zhejiang University of Technology, Hangzhou 310014, China

* Correspondence: icewater@zjut.edu.cn

Abstract: Silicon nitride ceramic balls are the key basic components of bearings in major equipment. Their key performance indices are accuracy and batch consistency. A grinding method with the most appropriate comprehensive performance is the basis and guarantee for optimizing these performance indices. In this study, an accurate wear model was established to predict the material removal rates (MRRs) of grinding methods and improve the dynamic grinding control ability of machinery during grinding, thus enabling the mass production of high-grade silicon nitride ceramic balls. A comprehensive analysis of various grinding and polishing methods revealed that the factors affecting sphericity were mainly manifested by the increase in ball sliding and the improvement in MRRs. Moreover, the three-body coupling grinding mode was considered as the grinding mode that was most applicable to silicon nitride ceramic balls. The upper disk served as an external nonlinear load, and the combination of the rotating speeds of the inner and outer disks of the lower grinding disk could actively control the ball's angle of rotation. This three-body wear mode can fully envelop the grinding trajectory and ensure uniform grinding. The traditional two-body wear model was unsuitable for three-body coupling grinding. A wear model based on three-body wear was established to predict MRRs and understand the principle of material removal in the grinding of precision spheres. Theoretical analysis and experimental verification revealed that the MRRs of silicon nitride ceramic balls during wear are not only related to the process parameters of external load and speed but also to the physical properties and geometric parameters of balls, abrasives, and processing machinery. The wear model results of silicon nitride ceramic balls in the three-body coupling grinding mode can be obtained stably on the basis of the established wear model by removing adverse effects and adopting optimized processing parameters, thus verifying the correctness of the theoretical and simulation analyses.

Keywords: three-body coupling grinding mode; silicon nitride ceramic balls; three-body wear; material removal rate; sphericity



Citation: Yu, W.; Lv, B.; Yuan, J. Wear Model of Silicon Nitride Ceramic Balls in Three-Body Coupling Grinding Mode. *Appl. Sci.* **2023**, *13*, 5796. <https://doi.org/10.3390/app13095796>

Academic Editors: Arkadiusz Gola, Izabela Nielsen and Patrik Grznár

Received: 6 March 2023

Revised: 1 May 2023

Accepted: 4 May 2023

Published: 8 May 2023



Copyright: © 2023 by the authors. Licensee MDPI, Basel, Switzerland. This article is an open access article distributed under the terms and conditions of the Creative Commons Attribution (CC BY) license (<https://creativecommons.org/licenses/by/4.0/>).

1. Introduction

Precision spheres are the core and basic components of roundness measuring instruments, gyroscopes, precision bearings, ball screws, ball guide rails, and precision measuring instruments, which are in great demand and widely used in precision machinery, the petrochemical industry, military defense, aerospace applications, and other fields. Due to its high hardness, wear resistance, low density and thermal expansion coefficient, excellent high-temperature resistance, non-magnetic quality, corrosion resistance, high thermal conductivity, self-moistening, and excellent thermal shock resistance and oxidation resistance, silicon nitride (Si_3N_4) is the preferred material for bearing balls at high temperatures, high speeds, high precision and in a special environment. It is widely used in wind turbines, high speed precision spindles, high temperature engines, and other fields [1–7]. The precision and batch consistency of spheres greatly affect the performance of functional precision parts [8–11]. The demand for precision spheres is increasing in industrial applications, such

as precision instruments and precision machine tools, and complete sets of batch processing technology and equipment for high-efficiency precision spheres are urgently needed.

All developed countries are working hard to study new methods and processes to achieve new breakthroughs for further elevating ultra-precision machining technology. The 14th Five-Year Plan for China's machinery industry also proposes considerably improving the design and technical level of major technical equipment and markedly enhancing the international competitiveness of products. In particular, the bottleneck of key parts that restrict the development of high-end equipment should be broken. The development of precision balls, which are the key parts of supporting components in high-end equipment, is particularly important. In recent years, the market demand for precision balls has increased at a rate of 15% and reached approximately 80 billion in 2021.

The batch processing of precision balls mainly follows the traditional steel ball processing method (V-groove processing method), during which the spin angle of the balls is constant [12]. The processing orientation is changed through the random movement of the circulation slot and is followed by repeated circular processing [7], which leads to low processing accuracy and poor batch consistency. Usually, precision balls are picked individually from batch-processed balls; this situation has been a difficulty perplexing the domestic and foreign fields of precision balling processing [10,11]. Moreover, production has a low automation degree and its process is affected by human factors [13–19].

On the basis of the National Natural Science Foundation project "Basic Research on New Grinding Method of Precision Ball" and "Basic Research on Advanced Ceramic High-efficiency Precision Machining Technology", the project team originally proposed a three-body coupling grinding method that could realize the ultra-precision grinding of balls and ensure the high precision, batch diameter variation, and batch consistency of precision ball machining in accordance with the balling principle, as shown in Figure 1.

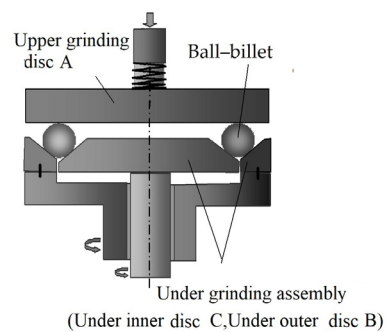


Figure 1. Principle of the double-rotation grinding equipment.

The three-body coupling grinding method aims to control the change in the rotation angle ($[-90^\circ, 90^\circ]$) of the ball blank actively by controlling the combination of the rotation speeds of the inner and outer grinding disks, such that the grinding trajectory covers the whole spherical surface evenly, achieving uniformity of the grinding trajectory on the machined spherical surface [20], effectively correcting the spherical error of the spherical surface from the balling principle, and improving the machining accuracy and batch consistency of the whole spherical surface. In previous research, the curves of inner disk rotation speed (Ω_C) and outer disk rotation speed (Ω_B) in the lower grinding disk were selected, as shown in Figure 2, and the grinding trajectory of the spherical surface in the three-body coupling grinding mode was obtained via simulation, as illustrated in Figure 3a. The mode when the rotation speeds of the inner disk and the outer disk of the lower grinding disk are always the same is equivalent to the traditional V-groove grinding mode. The simulated grinding trajectory is shown in Figure 3b. The grinding trajectory of the three-body coupling grinding mode is all over the spherical surface, whereas that of the traditional V-groove grinding mode presents a girdle pattern. The related work completed by the project has proven the feasibility of the three-body coupling grinding method to a considerable extent [20–26].

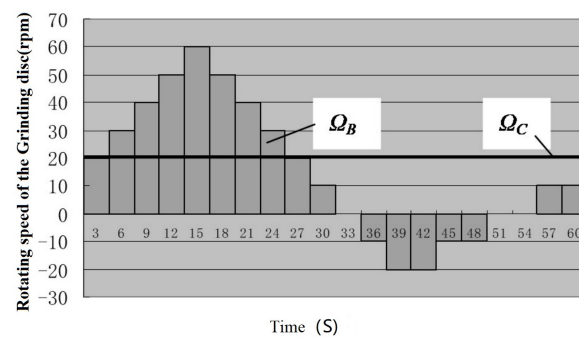


Figure 2. Variation curve of the lower disk rotation speed.

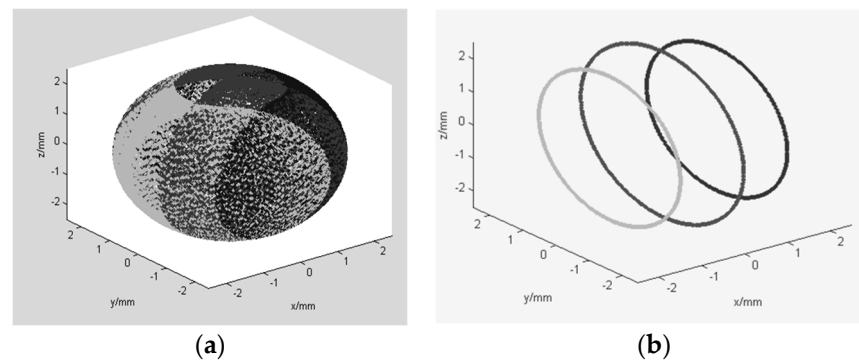


Figure 3. Computer-simulated grinding trajectory distribution [20–23]: (a) spherical grinding trajectory in the three-body coupling grinding mode; (b) spherical grinding trajectory in the V-groove mode.

In practice, however, numerous factors affect grinding accuracy. These factors include changes in processing conditions or the structural errors of grinding equipment, such that the ball does not move in the way predicted by theory during movement, which affects machining accuracy. In order to solve these problems, the factors that were more important to the grinding uniformity and material removal in actual processing were chosen and theoretically analyzed individually starting with the grinding uniformity and material removal amount that affected the balling accuracy, and their influencing laws on grinding uniformity and material removal were deduced to further ensure that precision ball processing in the three-body coupling grinding mode could obtain high accuracy and batch consistency stably and efficiently.

2. Comprehensive Performance Analysis of Precision Ball Grinding Methods at Home and Abroad

Many scholars have proposed numerous new processing methods in accordance with the characteristics of ball processing to reduce the cost and improve the accuracy, efficiency, and consistency of ball processing. These methods include the rotation angle actively controlled grinding method, three-body coupling grinding method, and magnetic fluid grinding method (MFP) [20–26].

2.1. Traditional V-Groove Grinding Method

The processing of various spheres mainly follows the V-groove grinding method for steel ball processing. The mechanism of this method is presented in Figure 4a. In this grinding method, the value of the rotation angle only depends on the diameters of the ball and the groove of the lower grinding disk and is independent of the rotation speed of the grinding disk; it remains almost unchanged during machining because it is very small [27–41]. The ball can only perform the grinding movement with constant relative orientation (the angle between the rotation axis and revolution axis of the ball is constant),

and the contact points between the ball and the grinding disk form a set of grinding trajectories on the surface of the ball with the rotation axis of the ball as the center.

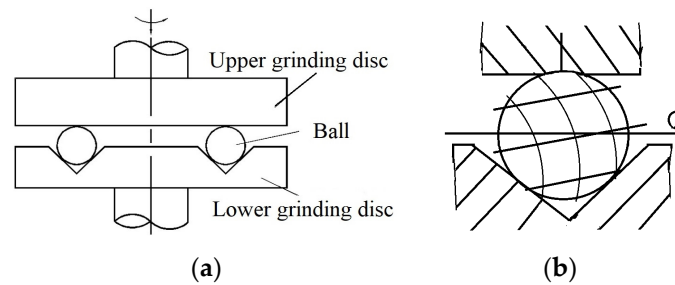


Figure 4. Traditional V-groove grinding mode: (a) schematic of the traditional V-groove grinding method; (b) grinding trajectory in the traditional V-groove grinding mode.

2.2. Rotation Angle Actively Controlled Grinding Mode

Kurobe et al. from Kanazawa University, Japan, proposed a rotation angle actively controlled grinding method (also known as the coaxial three-disk grinding method, as shown in Figure 5) [30–40]. In this method, the lower grinding disk in the V-groove grinding method is separated at the V-groove, such that the whole mechanism consists of three independently rotatable grinding disks. The rotation angle of the ball blank is adjusted by controlling the rotation speed changes of the three grinding disks. In this grinding mode, the rotation angle θ is not only related to geometric parameters, such as the diameter of the grinding disk and the included angle of the groove of the lower disk, but also to the rotation speed of the grinding disk. By adjusting the rotation speed, the value can be taken in the whole range of $[-90^\circ, 90^\circ]$, and the ball blank can execute a grinding movement with variable relative orientation. The grinding trajectory is a spatial spherical curve (Figure 6) with the rotation axis of the ball blank as its axis, which can cover the whole surface of the ball blank. The grinding disk grinds the ball blank in a scattered manner, which is beneficial to the uniform and efficient grinding of the ball blank surface. The experimental results show that this machining method can obtain good machining accuracy and efficiency; however, its application in production is limited by the complex mechanism of the grinding device.

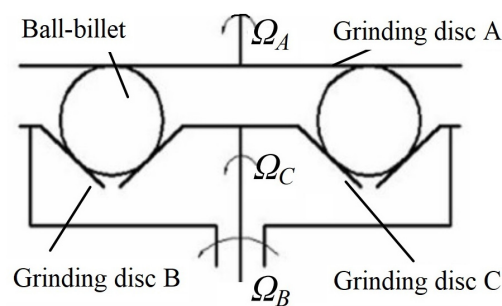


Figure 5. Schematic of the active control of the rotation angle.

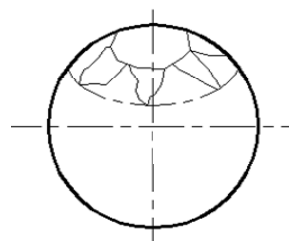


Figure 6. Grinding trajectory with the active control of the rotation angle.

2.3. Three-Body Coupling Grinding Mode

Although the rotation angle actively controlled grinding method can adjust the rotation angle of the ball to achieve a uniform machining trajectory by controlling the rotation speed changes of three independent rotating grinding disks, its structure is complicated. To reduce the complexity of the mechanism and the power source of the grinding equipment, the team of the Ultra-precision Machining Research Center of Zhejiang University of Technology improved the grinding mode on the basis of the active control of the rotation angle; combined it with the process control of the rotation speed change of the grinding disk; and proposed a three-body coupling grinding mode, the principle of which is shown in Figure 7 [23].

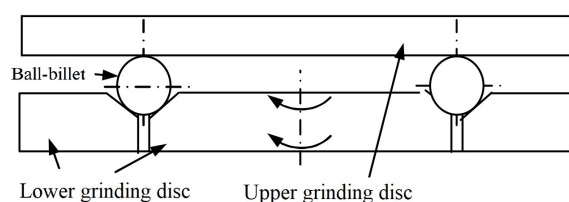


Figure 7. Schematic of the three-body coupling grinding mode.

In this grinding mode, the upper grinding disk does not need to rotate. The relative orientation of the ball's rotation and revolution axes can be adjusted by controlling the rotation speed changes of the inner and outer disks of the lower grinding disk, such that the grinding trajectory evenly covers the ball surface, thus achieving efficient and high-precision ball grinding. Given that the number of driving and transmission devices is reduced from three to two, the structure of the equipment can be greatly simplified, and the precision requirements of processing and assembly are relatively reduced. Therefore, the rotation angle can be continuously changed within the range of $[-90^\circ, 90^\circ]$. In addition, the grinding trajectory can cover the whole ball to significantly improve the processing accuracy in the mass production of precision balls. This effect is highly suitable for the small-batch production of precision balls; meets the increasing demand for precision balls; and further compensates for the defects of the traditional processing method, such as low efficiency and high costs [37].

Lv et al. and Yuan et al. [20,32] analyzed the rotation angle actually controlled grinding mode and discovered that the driving of the upper grinding disk in the grinding device was redundant and that the rotation of the upper grinding disk only increased by a relative movement velocity. A new grinding method—the three-body coupling grinding device—was proposed to reduce complexity. Figure 1 provides a schematic of the grinding structure of the three-body coupling grinding method. The upper grinding disk is under motion redundancy. The grinding movement with variable relative orientation can be realized just by controlling the rotation speed change of the lower inner and outer grinding disks, such that the grinding trajectory is evenly distributed on the ball surface. The high-efficiency and high-precision grinding of the ball blanks can thus be realized. Given that the number of driving and transmission devices is reduced from three to two, the structure of the equipment can be greatly simplified, and the precision requirements of processing and assembly are relatively reduced. This effect is highly suitable for the small-batch production of high-precision ceramic balls. Lv et al. [20] manufactured silicon nitride ceramic balls with high precision (roundness: $<0.05 \mu\text{m}$, surface roughness: $R_a < 5 \text{ nm}$) by combining key technology and newly developed processing equipment.

In 1984, Tani and Kawata [33] proposed using the MFP for facilitating the efficient grinding of precision spheres. This method has been improved by many scholars [40,41] and has greatly enhanced the machining efficiency of precision spheres. Its principle is illustrated in Figure 8. This method uses a magnetic fluid abrasive. When a magnetic field is imposed, the magnetic fluid pushes the floating disk upward and loads the ball. The high-efficiency machining of precision balls can be realized as a result of the very high shaft

rotation speed (above 10,000 rpm). However, this method has limited applications due to the high cost and short service life of magnetic fluids. Childs et al. [35–37] developed a non-MFP method for ceramic balls (Figure 9), in which the magnetic fluid is replaced with a cheap mixture of water and glycerol, the grinding disk is replaced with a resin-bonded diamond grinding wheel, and the self-adaptive supporting force is generated by a coil spring. Experiments demonstrated that the machining efficiency of this method is equivalent to that of magnetic fluid grinding, and the material removal rate (MRR) can be kept stable during machining [20–26].

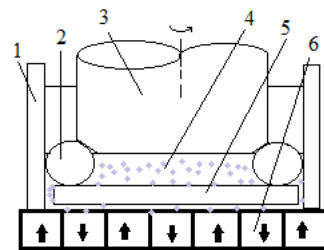


Figure 8. Schematic of the magnetic fluid structure. 1—grinding groove; 2—ceramic ball blank; 3—driving shaft; 4—mixture of magnetic fluid and abrasive; 5—floating plate; 6—magnet.

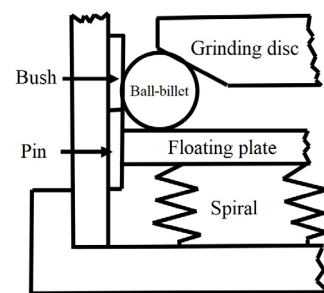


Figure 9. Schematic of the non-magnetic fluid structure.

The above analysis illustrates that the three-body coupling grinding method has obvious comprehensive advantages in terms of machining accuracy, machining efficiency, and mechanical structure (Table 1).

Table 1. Comparison of the advantages and disadvantages of different grinding modes.

Grinding Mode	Grinding Efficiency	Grinding Accuracy	Mechanical Structure
Traditional V-groove grinding mode	Low	Low	Simple
Double V-groove grinding mode	High	High	Complicated
Magnetic fluid grinding mode	Very high	Low	Complicated
Rotation angle actually controlled grinding mode	High	High	Complicated
Three-body coupling grinding mode	High	High	Relatively simple

3. Analysis of the Wear Performance of Precision Spheres

The ball surface grinding trajectory equation of the traditional V-groove grinding method was derived using ball kinematics and developed into a grinding trajectory equation suitable for other grinding methods [42]. This equation has considerable guiding importance for the research and analysis of grinding methods.

3.1. Material Removal Mechanism of Precision Spheres

Ball grinding is a process of removing materials by using abrasive particles to decrease ball diameter, improve sphericity, and reduce surface roughness. Any cross-section of an

ideal sphere is a perfect circle, which is the starting point of the design of ball grinding methods. The grinding tool moves relative to the ball (Figure 10) such that the grinding trajectory is evenly distributed on the surface of the ball blank. This situation is the geometric condition for grinding materials into a ball. A physical condition for balling is that the amount of material removed from the surface of the ball can vary with spherical deviation or can be expressed as the following two points [20–23]:

(1) Equal probability of cutting: The cutting probability of every point on each spherical surface is the same.

(2) Size selectivity: In machining, large balls are ground, whereas small ones are not ground or are ground minimally. Grinding is performed along the direction of the long axis and is not performed or is lessened along the direction of the short axis.

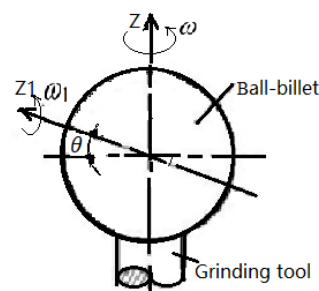


Figure 10. Schematic of balling.

Combining the basic balling conditions and the machining process shows that the factors that affect balling accuracy can be classified into two aspects: the uniformity of the grinding trajectory and MRR. Previous research shows that the uniformity of the grinding trajectory is more important than other factors and that MRR is subordinate [23]. Therefore, this study explored the influencing factors of grinding uniformity and their final influence on sphericity with the expectation of providing theoretical and technical support for actual production.

3.2. Status of Research on the Wear Model of Silicon Nitride Ceramic Balls

The surface energy of ceramic balls is low, and the adhesion of grinding media and abrasives is poor. It affects the machining efficiency, surface roughness, and batch diameter variation of ceramic balls. The dimensional accuracy and surface quality of ceramic balls have a very significant impact on the life of shaft bearings, and the pursuit of dimensional accuracy and surface quality will significantly increase the manufacturing cost, so it is of great significance to study high efficiency and low-cost ceramic ball grinding and polishing processing technology. A gentle process with a high removal rate is needed to minimize surface damage and achieve high polishing speeds. This process is called magnetic float polishing (MFP). It was originally developed by Tani and Carvatta [39], then greatly improved by Meiyuan and Kato [40], Childs et al. [43–45], Raghunandan et al. [41,46], and Komandruri et al. [47,48] by adding a float to generate a uniform and high polishing force. Zhang and Childs [49–51] developed a non-magnetic fluid grinding process for ceramic balls. In this process, ceramic balls are supported by springs instead of a magnetic force. They also discussed the grinding ratio, magnetic force cost, and non-magnetism. Chemical mechanical polishing (CMP) was also introduced. Vora et al. [52] and Uematsu et al. [53] demonstrated the feasibility of polishing silicon nitride via chemical mechanical grinding with iron oxide. Suga et al. [54], Kikuchi et al. [55], Ming J., and R. Komanduri et al. [56] studied CMP with various abrasives and discovered that chromium oxide is the most suitable abrasive for polishing silicon nitride. Bhagavatula and Komanduri [57] analyzed the principle of material removal using a chromium oxide abrasive in finishing silicon nitride ceramic balls.

Wei W. X. et al. investigated the micro-frictional wear characteristics and damage behaviors of silicon nitride ceramic balls and ball bearing steel [58]. Zhang K et al. concluded

that grinding speed and pressure have great influences on the removal method and the surface defects and surface quality of ceramic balls [59].

Childs et al. [44,45] also discussed ball blank movement and MRR. The volume removal rate dV/dt of the ball blank, which depends on the sliding speed U_s , was established on the basis of two-body wear, and the contact load W and the hardness Hv of the ball blank were decided by the abrasive wear principle (with K , the wear coefficient, being approximately 0.06):

$$\frac{dV}{dt} = \frac{K}{Hv} W U_s. \quad (1)$$

The above model is based on the fact that the embedded abrasive is located in the shaft surface. It indicates typical two-body wear, which is only related to process parameters and the hardness of the ball blank. In this study, the wear mode was reinvestigated, and a new three-body wear model based on the three-body coupling grinding mode was established to describe the interaction among the wafer, abrasive, and tool. The model is based on the normal distribution of the abrasive particle size on the ball blank–abrasive–tool interface and the plastic contact on the ball blank–tool interface.

4. Wear Mode of Silicon Nitride Ceramic Balls during Grinding

4.1. Wear Classification

In general, microscale wear is a two-body wear process when the abrasive is embedded in the counter-face but is a three-body wear process when abrasive particles are not embedded and can roll between two surfaces [60,61]. The three-body process is defined in the wear system. For two-body wear, the first body is the wear of greatest concern, and the second body is the counter-face that moves relative to the first body and directly or indirectly makes contact with the first body such that force can be transmitted between the two bodies. In three-body wear, the first and second bodies are as mentioned above, and the third body, which is composed of any solid material, is completely separated from the first two bodies and may appear on the contact surface between the first and second bodies.

In recent research, the abrasive wear process in which particles are fixed to the counter-face is described as groove abrasive wear, whereas the abrasive wear process in which abrasives can roll between two surfaces is described as rolling abrasive wear. Groove abrasive wear and rolling abrasive wear are used to replace two-body wear and three-body wear, respectively. For an effective abrasive wear process, the abrasive particles or the same area with a rough surface must remain in contact with the worn surface throughout the process. The worn surface caused by groove wear is characterized by grooves and is parallel to the sliding direction. The abrasive wear process in which the area of wear particles contacts the wear surface is constantly changing. The worn surface caused by rolling abrasive wear features severe deformation, multiple dented surfaces, and little or no directionality. The typical surfaces of the two wear processes are depicted in Figure 11.

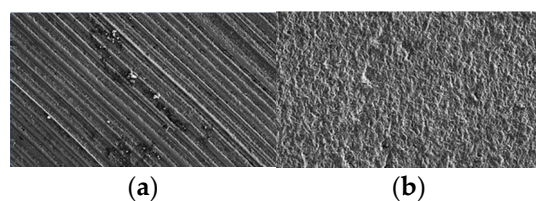


Figure 11. (a) Typical SEM surface image obtained after two-body wear; (b) typical SEM surface image obtained after three-body wear [60].

4.2. Conversion between Two-Body Wear and Three-Body Wear

The micro-scale wear test (also known as the indentation abrasive wear test of ball blanks), in which one ball blank rotates around the sample in the presence of fine abrasive slurry, is currently the standard wear resistance test of coating film processing in the project [61] funded by the European Union.

Figure 12 shows that the ball blank is sandwiched between coaxial rods and driven by a motor. A flat sample is vertically mounted on the rotating arm and loaded by the static weight suspended on the horizontal shaft against the ball.

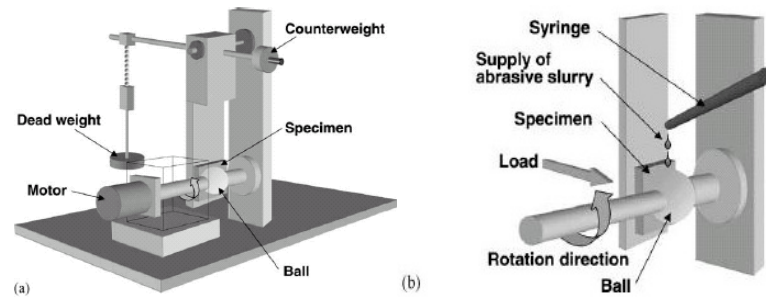


Figure 12. Schematic showing the details of (a) the experimental apparatus and (b) the contact interface and grinding slurry supply.

In the micro-scale wear test, the dominant wear mode is influenced by the external load, volume fraction of the abrasive in the slurry, wear materials, materials of the ball blank and sample, and surface conditions of the ball blank [60,61]. For all tested abrasives, the two-body groove wear mechanism is dominated by a high load and/or low slurry concentration. The mechanism dominated by a low load and/or high slurry concentration is a three-body process, in which abrasive particles are not embedded but are rolling between two surfaces, producing a severely deformed and multidented worn surface, and no obvious surface directionality exists. At a moderate load and/or slurry concentration, some wear marks present mixed characteristics, with a two-body groove in the center and three-body rolling around.

4.3. Wear Mode of Silicon Nitride Ceramic Balls

The wear conditions in the micro-scale wear test are similar to those in the grinding of silicon nitride ceramic balls. Therefore, the previous research conclusions are also applicable to the wear mode classification of silicon nitride ceramic balls in grinding processes.

Silicon nitride ceramic balls were ground under different conditions. Figure 13 shows the SEM surface images of ground silicon nitride ceramic balls [62]. These images illustrate that the dominant wear mode of the ball blank is the three-body (rolling wear) wear mode instead of the two-body wear mode. Studies have also shown that when fragile materials are used, plastic deformation occurs through dislocation. Therefore, a new model must be built to optimize the wear form of the old model on the silicon nitride ceramic ball.

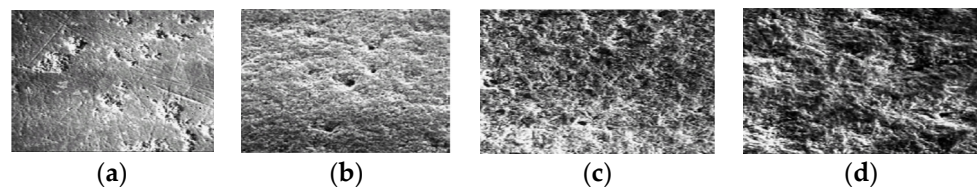


Figure 13. SEM surface images of silicon nitride ceramic balls ground under different conditions: (a) The load applied on a single ball blank was 4.5 N, and the abrasive particle size was W3.5; (b) 4.5 N, 180[#]; (c) 13 N, 180[#]; (d) 4.5 N, 80[#].

4.4. Three-Body Wear Model of Silicon Nitride Ceramic Ball Grinding

The three-body wear of fragile materials in grinding has been previously studied [63]. The removal rate, Z , which is defined as the height of materials removed per unit time, is given by the following formula:

$$Z = \alpha n \frac{P_i^{3/4}}{L_{m,c}} \frac{E_w^{5/4}}{K_{IC,w} H_w^2} p v, \quad (2)$$

where n is the number of the indentation points on the circumference of rolling particles; P_i is the normal load of each load-bearing particle; $L_{m,c}$ denotes the average size of load-bearing particles; E_w and H_w are the Young's modulus and hardness of the workpiece, respectively; K_{IC} is the fracture toughness of the workpiece; and p and v are the applied pressure and relative speed (sliding), respectively, which usually depend on the particle shape. For cone indentation, $\alpha = 0.01(\cos\psi)^{7/6}$ (ψ is the included angle of indentation points). Therefore, the MRR of silicon nitride ceramic balls can be obtained as follows:

$$MRR = Z \times A \times \rho_w = \alpha n \frac{P_i^{3/4}}{L_{m,c}} \frac{E_w^{5/4}}{K_{IC,w} H_w^2} p v \times A \times \rho_w = \alpha n \frac{P_i^{3/4}}{L_{m,c}} \frac{E_w^{5/4}}{K_{IC,w} H_w^2} W v \rho_w \tag{3}$$

In the Formula (3), $p.A = W$, where A is the interaction area between the ball blank and pad (in short, the tool surfaces, including the shaft, container, and float, are all called the pad here); W is the external load; and ρ_w represents the workpiece density.

Assuming that the concentration of abrasive particles in the contact zone is directly proportional to the volume fraction of the abrasive in the slurry provided, the load P_i carried by each abrasive particle (Figure 14) can be obtained from the following formula [62]:

$$P_i = \frac{\pi W D^2}{AcC_f} \tag{4}$$

where c is the proportionality constant, which varies with the abrasive type; C_f stands for the volume fraction of abrasives in the slurry; and D is the long axis of particles (for example, the diameter of abrasive particles).

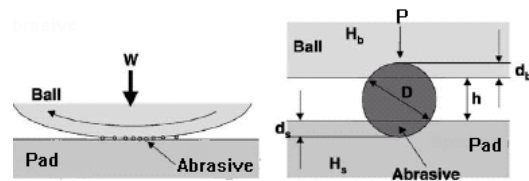


Figure 14. Model of the contact zone among the ball blank, sample, and abrasive.

Assuming that the macrodeformation of the ball blank and pad is elastic, and that the interaction zone A (Figure 15) is the upper zone when the spacing between the ball blank and pad is smaller than the diameter of abrasive particles, then A can be obtained using the following formula:

$$A = \pi a' = \pi (a^2 + 2R_b D) \tag{5}$$

where a is the radius of the Hertzian contact zone, and R_b denotes the radius of the ball blank. Hertzian contact circulates along the radius a as if it were caused by the contact of the ball blanks on the plane; $a = (0.75WR_b/E^*)^{1/3}$, where W is the load, E^* is the Young's modulus of the contact surface ($1/E^* = [1 - \nu_1]/E_1 + [1 - \nu_2]/E_2$), and ν_1 and ν_2 are the Poisson's ratios of the two contact materials.

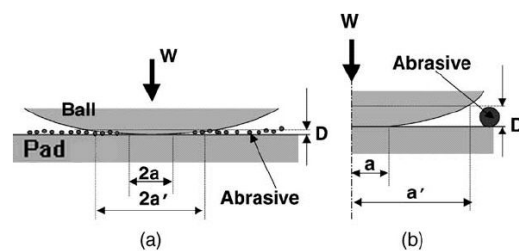


Figure 15. Model of the interaction zone principle. (a) Grinding structure diagram; (b) Local magnification diagram.

For the mean size $D = L_{m,c}$, the MRR of the ball blank can be solved in accordance with the formula

$$MRR = \alpha n \frac{L_{m,c}^{1/2}}{[(0.75WR_b/E^* + 2R_bL_{m,c})cC_f]^{3/4}} \frac{E_b^{5/4}}{K_{IC,b}H_b^2} W^{7/4} v \rho_b, \quad (6)$$

where E_b , H_b , $K_{IC,b}$, and ρ_w represent the Young's modulus, hardness, fracture toughness, and density of the ball blank, respectively.

5. Discussion

The above formula only calculates the MRR of one contact zone. However, in the three-body coupling grinding mode, three contact zones exist between the ball blank and pad. Therefore, the total MRR of a ball blank should be the sum of the MRRs of the three contact surfaces. The MRR formula consists of three parts.

5.1. Influence of Wear

The effects of geometrical α , n , size $L_{m,c}$, and concentration C_f are considered in this model. The lower limit of the average size of load-bearing particles is indirectly provided as $L_{m,c} \geq 2L_m$ (the average size of abrasive particles). The distribution of the abrasive particle size can satisfy the normal probability density function presented in a previous study [64]. C can be calculated via the possibilistic method:

$$c = \left[\int_{L_{m,c}}^{+\infty} \varphi(L) dL \right] / \left[\int_{-\infty}^{+\infty} \varphi(L) dL \right]. \quad (7)$$

When fine abrasive particles are used, especially in the polishing of the ball blank, three-body grinding is likely transformed into two-body grinding due to the ratio of the indentation height to the abrasive particle size [60,61].

5.2. Influence of the Material Properties of the Ball Blank and Pad

Stiffness, strength, and other properties of materials can affect the wear rate and friction coefficient, which is one of the main causes of wear [65–67]. The formula includes the size, Young's modulus, hardness, and fracture toughness of the pad. These factors are all constants for a certain material.

5.3. Influence of Process Parameters

The nonlinear correlation of the MRR with the external load of each ball blank shown in this model is related to the contact zone and abrasive indentation. The sliding speed is the most uncertain factor in the formula because the ball blank on the pad slides randomly. Childs et al. [44,45] analyzed the ball blank movement and load in the magnetic fluid grinding process in detail, as shown in Figures 16 and 17. The high removal rate is attributed to the high sliding speed between the ball blank and the driving shaft. Viscosity is the most important fluid variable to be controlled. Although high viscosity promotes a high sliding speed, excessive viscosity leads to a reduction in the removal rate.

5.4. Deficiencies of the Model

This study focused on the mechanical removal mechanism but did not discuss the chemical effect on MRR. Meanwhile, the degradation of the cutting ability of abrasive particles during ball grinding was not considered. A previous study [45] found that the removal rate would decrease with operation time. In addition, some factors that might affect the movement of the abrasive and ball blank, such as the shaft rotation speed, and the profile charts of the ball blank and pad, were ignored.

In view of these factors not being covered in this paper, we will specifically elaborate in two other papers to be published.

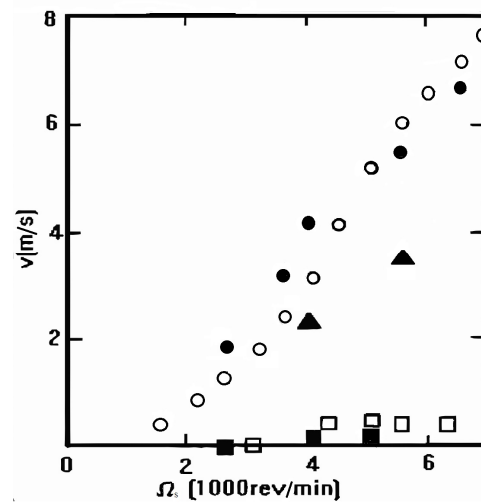


Figure 16. Skidding velocities at a load of 0.5 N for fluids. W1 (□) W2 (○) O1 (■) O2 (▲) O3 (●).

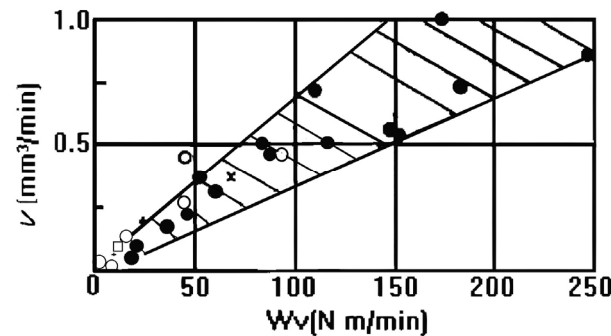


Figure 17. The dependence of the volume removal rate on WV for silicon nitride ground in fluids W1 (□) W2 (○) O3 (●).

5.5. Experimental Study on the Removal Form of Silicon Nitride Ceramic Spheres

The contact area of a silicon nitride ceramic ball and cast-iron disk was used in the experiment. The mechanical characteristics of the two are shown in Table 2.

Table 2. Mechanical properties of the Si₃N₄ ball and lapping plate employed in the experiment.

Parameter	Si ₃ N ₄ Ball Blank	Cast Iron Disk
Density (kg/m ³)	3200	7400–7700
Hardness (HV)	1500	230–250
Young’s modulus (Gpa)	310	113–157
Poisson’s ratio	0.26	0.23–0.27
Compressive strength (Mpa)	>3500	
Bending strength (Mpa)	600	>175
Surface roughness (Ra)	20 nm	

With different abrasive particle sizes, the relationship between wear form and load and abrasive particle concentration is basically consistent. That is to say, the material removal form may have little relationship with the abrasive size. That is to say, in addition to the mechanical and material characteristics of the wear device itself, the wear form mainly depends on the external load and abrasive concentration and has nothing to do with the particle size of the abrasive. Therefore, according to the ceramic wear experimental

conditions set in Table 3, different loads and different concentrations of grinding fluid in Table 4 were taken as conditions to test the material removal mode and corresponding MRR.

Table 3. Conditions of the ceramic ball abrasion test.

Abrasive grain	B ₄ C: W20, W7, W3.5
Lapping liquid base	Deionized water
Abrasive concentration	10–30 wt%
Load	0.5–2 N
Disc speed	20 rpm
Total speed of disc	500 rpm

Table 4. Values of MRR calculated in this study.

Load (N)	Concentration (wt%)					
	5	10	15	20	25	30
2	95.6	47.55	31.53	23.53	18.72 *	15.52 *
1.5	71.68	35.59	23.56	17.55 *	13.94 *	11.53 *
1	47.7	23.60	15.57 *	11.55 *	9.14 *	7.50 *
0.5	23.65	11.57 *	7.55 *	5.54 *	4.32 *	3.53 *

* Represents the removal of spherical material in triomeric form and mixed form.

6. Conclusions

In this paper, the application of a three-body coupled lapping method in the batch processing of silicon nitride ceramic balls was introduced. Then, based on the traditional two-body grinding model, the relevant parameters were analyzed, and the wear model of the three-body coupled grinding mode of silicon nitride ceramic precision balls was optimized. This model can be used to predict material removal during the grinding process of silicon nitride ceramic balls. The basic idea behind this model is $MRR = Z \cdot A \cdot \rho_b$. Compared with previous modeling methods based on the two-body wear model, this model not only combines the hardness, geometry, and fracture toughness of the ball billet itself, but also incorporates the abrasive concentration, mechanical motion, and structural parameters into the formula to predict the material removal rate. Through theoretical derivation and experimental verification, the appropriate load, abrasive concentration, and other related parameters can be given according to the model control, so as to obtain the required wear mode. The elimination of other adverse factors and the optimal design of the speed of the disk are also discussed in other articles.

Author Contributions: Conceptualization, W.Y. and B.L.; methodology, W.Y.; software, W.Y.; formal analysis, B.L.; investigation, B.L.; resources, J.Y.; data curation, W.Y.; writing—original draft preparation, W.Y.; writing—review and editing, W.Y.; visualization, J.Y.; project administration, J.Y. All authors have read and agreed to the published version of the manuscript.

Funding: This research was funded by [Public Welfare Program of Zhejiang Province] grant number [LZY23E050003], and [Natural Science Foundation of Zhejiang Province] grant number [LGG22F030013].

Institutional Review Board Statement: The study did not require ethical approval.

Informed Consent Statement: Not applicable.

Data Availability Statement: Not applicable.

Conflicts of Interest: The authors declare no conflict of interest.

References

1. Dezzani, M.M.; Pearson, P.K. Hybrid ceramic bearings for difficult applications. *J. Eng. Gas Turbine Surbines Power-Trans. ASME* **1996**, *118*, 449–452. [[CrossRef](#)]
2. Huang, C.; Yang, W.; Ai, X. The present situation and future prospect of study on advanced ceramic bearing. *China Ceram. Ind.* **1999**, *6*, 25–27.
3. Zhang, K. Analysis of NSK new rolling bearings in Japan. *Bearing* **2000**, *9*, 36–39.
4. Maeda, Y. Development of high precision silicon nitride balls. *Koyo Eng. J.* **2001**, *158*, 42–44.
5. Wang, G.Q.; Wang, Y.J. Research progress of ceramic ball bearings for spindle of high-speed CNC machine tools. *Bearing* **2003**, *9*, 41–59.
6. Furuma, K. Recent trends in research and development of rolling bearing at NSK. *Motion Control* **1996**, *1*, 5–12.
7. Rascher, R. Technical status and development trend of grinding steel ball. *Foreign Bear.* **1992**, *3*, 38–42.
8. Huang, B.W.; Kung, H.K. Variations of instability in a rotating spindle system with various bearings. *Int. J. Mech. Sci.* **2003**, *45*, 57–72. [[CrossRef](#)]
9. Xiao, X.L.; Yan, Q.S.; Lin, H.T.; Jiao, J.H.; Liu, J. Research progress of silicon nitride ceramic ball grinding and polishing technology. *J. Guangdong Univ. Technol.* **2018**, *35*, 18–23, 30.
10. Guo, W.G.; Yuan, J.L.; Xiang, Z.; Zhou, F.F.; Lv, B.M.; Zhao, P. Spheroidal Machining Test Based on Variable Turning Curvature Grinding Method with Single Turntable. *Surf. Technol.* **2018**, *7*, 252–258.
11. Guo, W.G.; Yuan, J.L.; Xiang, Z.; Lv, B.M.; Zhao, P.; Zhou, F.F. Experiment on process parameters for material removal of high-precision balls by spiral groove lapping plate. *J. Mech. Electr. Eng.* **2018**, *10*, 1058–1062.
12. Nie, L.F.; Zhao, X.J. Discussion on the rounding conditions of steel balls and its influencing factors. *Bearing* **2001**, *1*, 16–18.
13. Zhang, K.; Wang, H.; Sun, J. Simulation and experimental study on superfinishing silicon nitride full-ceramic ball bearing raceway. *Ordinance Mater. Sci. Eng.* **2019**, *4*, 49–54.
14. Chen, B.; Wei, Z.H.; Li, B.; Wang, Z.C.; Wang, T.F. Research and application progress of silicon nitride ceramics in four fields. *Bull. Chin. Ceram. Soc.* **2022**, *4*, 1404–1415.
15. Su, B.W.; Sun, B.Q.; Wang, Y.L.; Li, L.X.; Wan, L. Study on wear characteristics of water-borne silicon nitride all-ceramic rolling bearings. *Bearing* **2020**, *3*, 22–25.
16. Su, B.W.; Xin, S.H.; Ma, Y.; Ding, P.; Zeng, Y.P. Dynamic corrosion and wear behavior of silicon nitride all-ceramic rolling bearing in acidic aqueous solution. *Bearing* **2020**, *4*, 38–42.
17. Sun, H.X.; Cao, L.Y.; Wang, Z.H. Friction and wear properties of silicon nitride ceramic tool materials sintered by spark plasma. *Bull. Chin. Ceram. Soc.* **2019**, *12*, 3736–3742.
18. Wei, C.M.; Li, Y.B.; Jiang, C.Y.; Zhang, J.T.; Ding, P. Corrosion and wear characteristics of silicon nitride ceramics in acidic medium solution. *Bearing* **2019**, *8*, 22–25.
19. Zhong, J.; Li, C.S.; Li, J.F.; Hua, G.M. Preparation and characterization of silicon nitride ceramic composites reinforced by silicon carbide. *Bearing* **2019**, *1*, 36–40.
20. Lv, B.H. Research on Ceramic Balling and Sphere-Shaping Mechanism with Rotated Dual-Plates Machine. Ph.D. Thesis, Harbin Institute of Technology, Harbin, China, 2007.
21. Xu, Q. Research on the Technology of High Efficiency Lapping Method of Hard Material Sphere. Master's Thesis, Zhejiang University of Technology, Hangzhou, China, 2008.
22. Yang, F. The Research of Kinematic Characteristics of Balls and Their Influence Factors on the Rotated Dual-Plates Lapping Platform. Master's Thesis, Zhejiang University of Technology, Hangzhou, China, 2010.
23. Tao, B.C. Speed Optimization and Process Experiment Research on the Dual Rotating Plates Lapping Mode of the Ceramic Balls. Master's Thesis, Zhejiang University of Technology, Hangzhou, China, June 2006.
24. Tang, K.F. Study on the Mechanism of Grinding Achievement under Double Rotation Grinding Mode. Master's Thesis, Zhejiang University of Technology, Hangzhou, China, 2010.
25. Chen, J.J. Research on the Impact of the Spherulization Mechanism in the Process of Rotated Dual-Plates Lapping on Sphericity. Master's Thesis, Zhejiang University of Technology, Hangzhou, China, 2010.
26. Zhang, B.; Nakajima, A. Grinding of Si₃N₄ ceramic balls with the aid of photo-catalyst of TiO₂. *Ann. CIRP* **2002**, *51*, 259–262. [[CrossRef](#)]
27. Ido, M.; Hazi, T.; Nakazima, M. On the miniature ball bearings—On the effect of revolutionary radius in lapping steel balls. *Jpn. Soc. Precis. Eng.* **1960**, *26*, 470–475. (In Japanese) [[CrossRef](#)]
28. Ido, M.; Hazi, T.; Nakazima, M. On the miniature ball bearings—On the effect of lapping liquid in lapping steel balls (Part 2). *Jpn. Soc. Precis. Eng.* **1961**, *27*, 261–267. (In Japanese) [[CrossRef](#)]
29. Ido, M.; Hazi, T.; Nakazima, M. On the miniature ball bearings—On the lapping pressure in lapping steel balls (Part 1). *Jpn. Soc. Precis. Eng.* **1958**, *24*, 161–168. (In Japanese) [[CrossRef](#)]
30. Ren, C.Z. The eccentric circular groove lapping technique for ceramic balls. *Chin. J. Mech. Eng.* **1995**, *11*, 21–24.
31. Yuan, J.L.; Wang, Z.W.; Lv, B.H. Simulation Study on the Developed Eccentric V-grooves Lapping Mode for Precise Ball. *Key Eng. Mater.* **2006**, *304*, 300–304. [[CrossRef](#)]

32. Wang, Z.W. Fundamental Research on the Lapping Technology of Precise Balls. Master's Thesis, Zhejiang University of Technology, Hangzhou, China, 2005; pp. 27–35.
33. Kurobe, T.; Kakuta, H.; Onoda, M. Spin angle control lapping of balls (1st report)—Theoretical analysis of lapping mechanism. *J. Jpn. Soc. Precis. Eng.* **1996**, *62*, 1773–1777. [[CrossRef](#)]
34. Kurobe, T.; Kakuta, H.; Onoda, M. Spin angle control lapping of balls (2nd report)—Theoretical analysis of lapping mechanism. *J. Jpn. Soc. Precis. Eng.* **1997**, *63*, 726–730. [[CrossRef](#)]
35. Wang, J.; Zheng, H.W. A new method for grinding ceramic balls. *Diam. Abras. Eng.* **1996**, *4*, 15–18.
36. Wu, Y.H.; Zhang, K.; Sun, H. Rubbing process technology of HIPSN ceramic balls. *Key Eng. Mater.* **2001**, *202*, 185–188. [[CrossRef](#)]
37. Li, S.H.; Wu, Y.H. Mechanical analysis of new-style grinding method of ceramic balls. *J. Shenyang Archit. Civ. Eng. Univ.* **2003**, *18*, 229–232.
38. Lu, F.; Wu, Y.H.; Zhang, K. Technological investigation on taper grinding for hybrid bearing ceramic ball. *J. Northeast Univ.* **2004**, *25*, 82–85.
39. Tani, Y.; Kawata, K. Development of high-efficient fine finishing process using magnetic fluid. *Ann. CIRP* **1984**, *33*, 217–220. [[CrossRef](#)]
40. Umehara, N.; Kato, K. Principles of magnetic fluid grinding of ceramic balls. *Appl. Electromagn. Mater.* **1990**, *1*, 37–43.
41. Raghumandan, M.; Noori-Khajavi, A.; Umehara, N.; Komanduri, R. Magnetic float polishing of advanced ceramics. *Trans. ASME J. Manuf. Sci. Eng.* **1996**, *119*, 521–528.
42. Chen, M.C. Theoretical Analysis of Ball Dynamic Characteristics of Ball Grinding Machine. Master's Thesis, National Sun Yat-sen University, Taiwan, China, 2000; pp. 5–10.
43. Childs, T.H.C.; Yoon, H.J. Magnetic fluid grinding cell design. *Ann. CIRP* **1992**, *41*, 343–346. [[CrossRef](#)]
44. Childs, T.H.C.; Jones, D.A.; Mahmood, S.; Zhang, B.; Kato, K.; Umehara, N. Magnetic fluid grinding mechanics. *Wear* **1994**, *175*, 189–198. [[CrossRef](#)]
45. Childs, T.H.C.; Mahmood, S.; Yoon, H.J. Magnetic fluid grinding of ceramic balls. *Tribol. Int.* **1995**, *28*, 341–348. [[CrossRef](#)]
46. Raghunandan, M.; Komanduri, R. Finishing of silicon nitride balls for high-speed bearing applications. *Trans. ASME J. Manuf. Sci. Eng.* **1998**, *120*, 376–386. [[CrossRef](#)]
47. Umehara, N.; Komanduri, R. Magnetic fluid grinding of HIP-Si₃N₄ rollers. *Wear* **1996**, *192*, 85–93. [[CrossRef](#)]
48. Jiang, M.; Komanduri, R. On the finishing of Si₃N₄ balls for bearing applications. *Wear* **1998**, *215*, 267–278. [[CrossRef](#)]
49. Chang, F.Y.; Childs, T.H.C. Non-magnetic fluid grinding. *Wear* **1998**, *223*, 7–12. [[CrossRef](#)]
50. Child, T.H.C.; Moss, D.J. Grinding Ratio and Cost Issues in Magnetic and Non-Magnetic Fluid Grinding. *Ann. CIRP* **2000**, *49*, 261–264. [[CrossRef](#)]
51. Childs, T.H.C.; Moss, D.J. Wear and cost issues in magnetic fluid grinding. *Wear* **2001**, *249*, 509–516. [[CrossRef](#)]
52. Vora, H.; Orent, T.W.; Stokes, R.J. Mechano-Chemical polishing of Silicon Nitrided. *J. Am. Ceram. Soc.* **1983**, *65*, C140–C141. [[CrossRef](#)]
53. Uematsu, T.; Suzuki, K.; Wu, M.H.; Suzki, K.; Imanaka, O. Efficient Mechanochemical Polishing for Silicon Nitride Ceramics, Machining of Advanced Materials. *NIST Spec. Publ.* **1993**, *847*, 409–413.
54. Suga, T.; Suzuki, S.; Miyazawa, K. Mechanochemical Polishing of Sintered Silicon Nitride. *JSPE* **1989**, *55*, 2247–2253. (In Japanese)
55. Kikuchi, M.; Takahashi, Y.; Suzuki, S.; Bando, Y. Mechano-Chemical Polishing of Silicon Carbide Single Crystal with Chromium Oxide Abrasive. *J. Am. Ceram. Soc.* **1992**, *75*, 189–195. [[CrossRef](#)]
56. Nelson, M.J.; Wood, O.; Komanduri, R. On chemo-mechanical polishing (CMP) of silicon nitride (Si₃N₄) work material with various abrasives. *Wear* **1998**, *220*, 59–71.
57. Bhagavatula, S.R.; Komanduri, R. On the Chemo-Mechanical Polishing of Silicon Nitride with Chromium Oxide Abrasive. *Philos. Mag.* **1996**, *74*, 1003–1017. [[CrossRef](#)]
58. Wei, W.X.; Su, Y.F.; Fan, H.Z.; Liang, H.Q.; Song, J.J.; Zhang, Y.S.; Hu, L.T. Fretting Friction and Wear Characteristics and Damage Behaviors of Si₃N₄ Ceramic Balls Sliding against Bearing Steel. *Tribology* **2022**, *1*, 113–122.
59. Zhang, K.; Wang, D.; Li, S.; Sun, J.; Wu, Y.; Childs, T.H.C.; Mahmood, S.; Yoon, H.J. Material removal mode of lapping Si₃N₄ balls. *Diam. Abras. Eng.* **2019**, *39*, 38–44.
60. Trezona, R.I.; Allsopp, D.N.; Hutchings, I.M. Transitions between two-body and three-body abrasive wear: Influence of test conditions in the microscale abrasive wear test. *Wear* **1999**, *225*, 205–214. [[CrossRef](#)]
61. Adachi, K.; Hutchings, I.M. Wear-mode mapping for the micro-scale abrasion test. *Wear* **2003**, *255*, 23–29. [[CrossRef](#)]
62. Ren, C.Z.; Wang, T.Y.; Jin, X.M.; Xu, H. Experimental research on the residual stress in the surface of silicon nitride ceramic balls. *J. Mater. Process Technol.* **2002**, *129*, 446–450. [[CrossRef](#)]
63. Buijs, M.; van Houten, K. Three-body abrasion of brittle materials as studied by lapping. *Wear* **1993**, *166*, 237–245. [[CrossRef](#)]
64. Chauhan, R.; Ahn, Y.; Chandrasekar, S.; Farris, T.N. Role of indentation fracture in free abrasive machining of ceramics. *Wear* **1993**, *162*, 246–257. [[CrossRef](#)]
65. Zaghoul, M.Y.M.; Zaghoul, M.M.Y.; Zaghoul, M.M.Y. Physical analysis and statistical investigation of tensile and fatigue behaviors of glass fiber-reinforced polyester via novel fibers arrangement. *J. Compos. Mater.* **2023**, *57*, 147–166. [[CrossRef](#)]

66. Zaghoul, M.M.Y.; Steel, K.; Veidt, M.; Heitzmann, M.T. Mechanical and Tribological Performances of Thermoplastic Polymers Reinforced with Glass Fibres at Variable Fibre Volume Fractions. *Polymers* **2023**, *15*, 694. [[CrossRef](#)]
67. Zaghoul, M.M.Y.; Steel, K.; Veidt, M.; Heitzmann, M.T. Wear behaviour of polymeric materials reinforced with man-made fibres: A comprehensive review about fibre volume fraction influence on wear performance. *J. Reinf. Plast. Compos.* **2022**, *41*, 215–241. [[CrossRef](#)]

Disclaimer/Publisher's Note: The statements, opinions and data contained in all publications are solely those of the individual author(s) and contributor(s) and not of MDPI and/or the editor(s). MDPI and/or the editor(s) disclaim responsibility for any injury to people or property resulting from any ideas, methods, instructions or products referred to in the content.